Preoperative Virtual Surgery to Optimize Nasal Airflow

Stanley W. McClurg, MD[1], Francis Sheer, MS[2], Samir Ghadiali, PhD[2], Subinoy Das, MD[1]
[1]Department of Otolaryngology-Head and Neck Surgery, [2]Department of Biomedical Engineering

Introduction

Nasal airway obstruction is a common disease with high prevalence and significant social and economic burden. Nearly 9.5 million people annually present to their primary care physician with the chief complaint of nasal obstruction[1] and nasal obstruction is responsible for an estimated $6 billion in annual healthcare expenditures[2]. Over 340,000 septoplasties and/or turbinate surgeries are performed annually for nasal airway obstruction, making this the 3rd most common set of procedures performed by otolaryngologists[3]. While septoplasty and/or turbinate surgeries are often successful in relieving nasal airway obstruction, between 10 - 40% of patients complain of persistent obstruction after surgery [4,5,6,7]. This moderate failure rate is in part due to traditional physical exam interpretations from anterior rhinoscopy correlating poorly to the patient's sensation and probable 3D location of actual nasal obstruction. Furthermore, no objective measures of nasal airflow (such as acoustic rhinometry[8], rhinomanometry[9], etc) have been sufficiently accurate to be commonly used in clinical practice to aid the otolaryngologist in surgical planning. The development of an accurate objective measure that strongly predicted the locations of anatomic nasal obstruction would be a great aid to improving the quality of nasal airway surgery and reducing the overall failure rate. In addition, this accurate objective measure could reduce the incidence of unnecessary surgery and help personalize and minimize operations for each unique patient. With the advances in computing processing speed in recent years, we endeavored to use computational fluid dynamic analysis of 3D reconstructions of nasal airways from computed tomography images as a method for developing precise calculations of nasal airflow for individual patients. Furthermore, this approach also provides the added benefit of allowing the surgeon to perform pre-operative virtual surgery on the 3D reconstructions to optimize nasal airflow and create a personalized surgical plan for each particular patient. Here, we describe our collaborative efforts within the otolaryngology, biomedical engineering, and supercomputing disciplines to develop these software algorithms and the successful use of this approach with an actual patient with nasal obstruction.

Materials and Methods

3D models of the sinonasal cavities of the patient was reconstructed from sinus CT volumetric voxel data from the nares anteriorly to the nasopharynx posteriorly. Images were taken on a 3D Accuitomo XYZ Slice View Tomograph (J. Morita MFG. Corp). After the images were obtained, thresholding and segmentation were performed in a custom-programmed MatLab (Natick, MA) routine. The customized program allowed the surgeon to process each image (correlating to a computed tomography coronal slice) individually or process images in blocks using the same parameter set. After the images were segmented, results were outputted in two different formats: 1) the domain was meshed, and the finite element mesh was outputted and 2) a 3D stereolithography (STL) file of the reconstructed geometry was outputted. Due to the negligible effect on overall airflow resistance, the sinuses were removed from the computational domain.[10,11,12]

A 3D reconstruction of the nasal airway was then created to allow the surgeon to interactively manipulate the anatomy of the nasal cavities. The surgeon could simulate a large variety of procedures, including: limited septoplasty, unilateral or bilateral submucous resection of the inferior turbinates, and concha bullosa excision of the middle turbinates. The virtual surgery is performed by allowing the surgeon to maneuver through the image stack, changing the region of interest on each subsequent image to either bone or tissue (black) or air (white).

Airflow patterns in the nasal airways are governed by two main factors: nasal geometry and flow rate. As shown in previous literature, we assumed laminar flow models in our CFD flow models associated with quiet breathing (5 to 12 L/min) when performing CFD within the nasal passages[13,14,15,16] Once the flow rate exceeds 20 L/min, as during light exercise or sniffing, nasal airflow becomes turbulent. In this study, only quiet breathing rates were considered, therefore, the flow was chosen to be modeled as incompressible and laminar. Also for this study, steady state inspiration was modeled.

Results

The selected patient was a Caucasian, 47-year-old female who presented to our office with a history of significant nasal obstruction and recurrent sinusitis. A CT scan of the nasal passages was performed, and showed inferior turbinate hypertrophy and a significant septal deviation. Before the patient underwent surgery, the surgeon performed a 'Virtual Surgery' on the patient conducting the planned procedures scheduled to be performed during the true surgical intervention. The entire processing time required to perform the virtual surgery and computational fluid dynamics for this patient was four hours 55 minutes. The patient then underwent the planned surgical intervention which included a septoplasty and bilateral submucous resection of the inferior turbinates.

One month post-operatively, the patient underwent a post-operative CT scan of the sinuses. Figure 2 shows a comparison of images from the various states of the patient.

Figure 2A represents the original CT image of the patient. Figure 2B shows the segmented images of the CT scan shown in A (black is bone/soft tissue; white is air). Figure 2C shows a segmented image after virtual surgery was performed on the patient. In the image, the septal deviation has been resected and the inferior turbinates have been reduced. Figure 2D shows a segmented image of the same coronal slice that has been reconstructed from the actual post-operative CT scan.

Figure 3 represents the particle flow diagrams of this patient pre-operatively and post-operatively.

The resulting calculated nasal airflow resistances are represented in Figure 4.

Figure 1

Virtual Nasal Surgery Algorithm

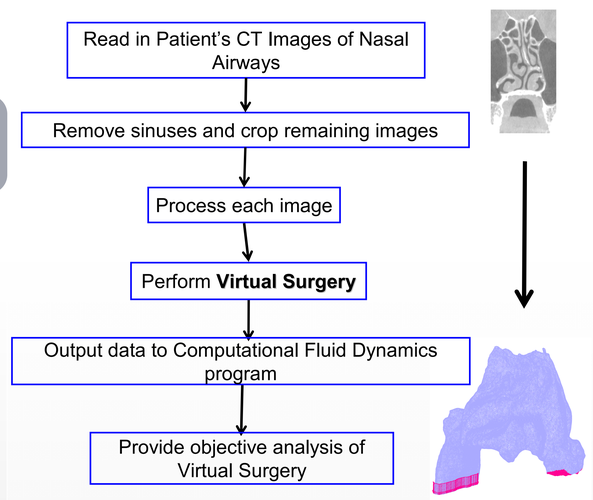

Figure 2

Cross-sectional Images of Virtual Surgical Planning System

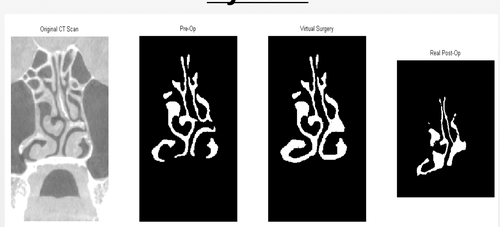

Original CT scan | Pre-op reconstruction | Virtual Surgery | True Post-op reconstruction

Figure 3

Computational Fluid Dynamics Particle Trace Plots

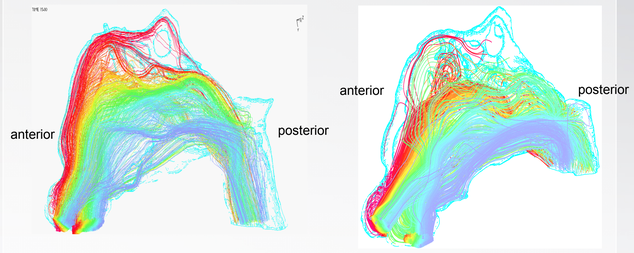

Pre-op | Post-op

Figure 4

Nasal Airflow Resistance Plots

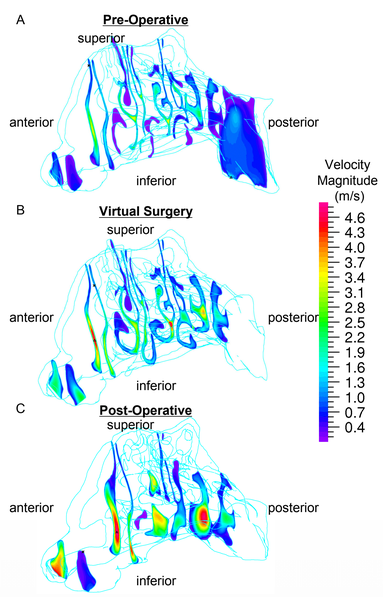

Table 1: Comparison of Pre-operative, Virtual Surgery, and Post-operative Nasal Resistances

	Pre-Op		Virtual Surgery		Post-Op	
	Left	**Right**	**Left**	**Right**	**Left**	**Right**
Resistance Value (Pa*s/mL)	**0.42**	**0.19**	**0.21**	**0.12**	**0.29**	**0.08**
Total Resistance (Pa*s/mL)	**0.13**		**0.08**		**0.06**	
Percent Decrease	**N/A**		**39.8%**		**50.5%**	

Discussion

This technique provides a systematic route to obtain a pre-operative surgical plan for patients with anatomic causes of nasal obstruction. The use of computational fluid dynamics to assist the surgeon is computationally intensive; however, given current advances in computing power, the entire process in this pilot study with the use of commonly available computing workstations was completed in under 5 hours for this patient.

The concept of nasal computational fluid dynamics was first described by Proetz in 1941[17]. This initial research described the laminar and turbulent airflow dynamics of the airflow path through the sinonasal cavity. Air initially enters the vestibule, flows through the internal nasal valve, is then directed superiorly towards middle turbinate, turns medial as well as lateral to the middle turbinate, and then is directed to the posterior choana. Any deviation to this pattern from anatomical deviations has the potential to cause changes in the turbulent and laminar patterns of nasal airflow, in turn, causing either increased airflow resistance, or the perception of nasal congestion. A significant benefit of this model is that the continuous acquisition of objective data correlated to subjective, validated outcome measures, can start to better define the reference ranges of normal airway resistance.

Our proposed algorithm represents a logical next step in utilizing CFD for pre-operative surgical analysis for patients with nasal congestion and found to have anatomic obstruction. Currently, this technique assesses the nasal anatomy obtained at a single instant (when the CT was obtained) and is not dynamic. Therefore, the dynamic nature of the nasal cycle and internal and external nasal valves are insufficiently addressed. The advent of point-of-care CT scans with rapid image acquisition may allow for multiple image sets to be taken (pre-decongestion and post-decongestion), similar to flexion-extension xrays for spine mobility, etc, and help improve the dynamic assessment of nasal airway resistance. Furthermore, airspace in the paranasal sinus cavities, typically negligible for airway resistance, was deleted from the image stacks to reduce computational time required for analysis. CFD has accurately modeled airflow in closed systems with multiple moving variables such as the Eustachian tube, so it is predicted that enhanced versions of these software could address these important dynamic regions. The most significant obstacle to overcome in nasal airflow analysis lies in the fact that there is no current gold-standard technique to assess overall nasal resistance. Acoustic rhinometry[8] and rhinomanometry[9] have been proposed as nasal resistance measures. However, these techniques have not been standardized, and results have not been sufficiently correlated with patient symptomatic scores[21]. To assess the reproducibility and accuracy of our technique, future studies should address the correlation between virtual surgical nasal resistances and patient satisfaction scores. Complex areas of research that adequately address the dynamic nature of our nasal anatomy, the different flow phenomenon found in resting states versus heavy breathing states, and the sometimes poor correlation of true nasal resistance with subjective symptoms (such as that found in empty nose syndrome) will need to be performed. However, this pilot study reveals that CFD analysis and pre-operative virtual surgery may be a useful and potentially revolutionizing adjunct to current techniques used to diagnose and treat nasal airway surgery. Furthermore, CFD-containing algorithms could be readily incorporated into current image guidance technologies currently being used for sinus surgery. The exponential advancements in computing technology give hope that CFD analysis may be a viable and practical adjunct to nasal airway surgery in the near future.

Conclusion

We have developed a novel software algorithm and technique to pre-operatively perform virtual surgery on 3D reconstructions of patients undergoing nasal airway surgery and use objective airflow calculations from computation fluid dynamics analysis to objectively assess these potential surgical interventions. These techniques may allow the surgeon to optimize the surgical intervention for each specific patient, creating a personalized surgical approach to the patient with nasal obstruction, and significantly improving the long-term success rate of nasal surgical interventions.